Evolution of picosecond surface electric fields generated by photon-induced charge emission from $La_{0.67}Sr_{0.33}MnO_3$ films

Runze Li,[1,2,*] Pengfei Zhu,[1] Haijuan Zhang,[1] Yao Wang,[3] Jie Chen,[1] Peter M. Rentzepis,[2] and Jie Zhang[1,*]

[1]*Key Laboratory for Laser Plasmas (Ministry of Education), School of Physics and Astronomy, and Collaborative Innovation Center of Inertial Fusion Sciences and Applications (CICIFSA), Shanghai Jiao Tong University, Shanghai 200240, China*

[2]*Department of Electrical and Computer Engineering, Texas A&M University, College Station, Texas 77843, USA*

[3]*Department of Physics, Harvard University, Cambridge, Massachusetts 02138, USA*

(Received 27 February 2020; revised 4 June 2020; accepted 8 June 2020; published 1 July 2020)

In recent years, transient electric field is becoming a means for the generation of hidden states or phase transitions. In this study, the spatial-temporal distribution of picosecond surface electric fields, associated with the femtosecond-laser-induced charge emission from $La_{0.67}Sr_{0.33}MnO_3$ (LSMO) single-crystal films, were interrogated by subpicosecond electron pulses and reconstructed by a three-layer theoretical model. A strong picosecond surface electric field, on the order of 100 kV/m, was generated on LSMO films. Such self-induced transient electric fields may be a promising means for controlling ultrafast processes in materials.

DOI: 10.1103/PhysRevB.102.024302

I. INTRODUCTION

In strongly correlated materials, the interplay among electron, lattice, orbital, and spin degrees of freedom determines their unique electronic and magnetic properties, including superconductivity and colossal magnetoresistance effects [1]. As the equilibrium state properties of strongly correlated materials are extensively studied, particular interest has been placed on the nonequilibrium dynamics generated by means of ultrafast optical excitations [2–4]. However, those optical excitations usually lead to a variety of effects involving more than one degree of freedom. Previous studies of such ultrafast dynamics have been mainly focused on the energy relaxation of electron systems, electron-phonon couplings, and coherent phonon generations [5].

In the past few years, the strong THz sources, which are mainly generated by intense laser-matter interaction or free-electron lasers [6] have provided means for selectively exciting lattice vibrational modes through resonance absorption [7] and manipulating the spin degree of freedom of these materials through interaction with the THz electric fields [8]. Meanwhile, transient polarization modulation, owing to electric field bias effects of single-cycle THz pulse excitation, has been observed in thin $BaTiO_3$ ferroelectric films [9]. In $SrTiO_3$ crystals, a hidden state was observed recently [10]. It was also demonstrated that the orbital domains of thin films such as $La_{0.5}Sr_{1.5}MnO_4$ can be oriented by means of the polarized THz electric fields, which are on the order of hundreds kV/m [11].

The promising role of ultrafast transient electric fields, for the control of ultrafast events in complex oxide materials, suggests that it is important to continuously explore means for the generation of strong transient electric fields that are easily accessible for such applications. One potential candidate is the surface transient electric field (TEF) associated with femtosecond-laser-induced charge emissions. However, due to the lack of ultrafast electromagnetic field probes, the strength, transient distribution, and evolution of the TEFs generated during charge emission processes remain an open question.

In recent years, femtosecond electron pulses are becoming a powerful means for probing such TEFs and have revealed that picosecond transient electric fields could be generated on aluminum [12], silicon [13], and graphite [14] surfaces illuminated by femtosecond laser pulses with intensities well below the damage threshold. However, the spatial-temporal distribution of TEFs on complex oxide materials, excited by femtosecond laser pulses, has not been investigated. A typical example is the prototypical material $La_{1-x}Sr_xMnO_3$ ($0 < x < 1$), whose photoelectric effect measurements have been mainly focused on the transport properties of *p-n* junctions or heterostructures [15].

To this end, we characterize and reconstruct the spatial-temporal distribution of surface TEFs, generated by femtosecond laser pulse illumination of $La_{0.67}Sr_{0.33}MnO_3$ (LSMO) single-crystal films at two temperatures(300 and 77 K), using the combination of subpicosecond electron pulses and a three-layer model. A strong electric field, on the order of 100 kV/m and duration time of tens of picoseconds, was generated on the surface of a semimetal phase LSMO film at room temperature. This type of picosecond strong electric field may potentially serve as a means for the ultrafast control of such materials directly or through magnetoelectric coupling. The method and analyses presented in this paper may also be employed to evaluate other strongly correlated materials.

*Runze@tamu.edu; jzhang1@sjtu.edu.cn

 ©2020 American Physical Society

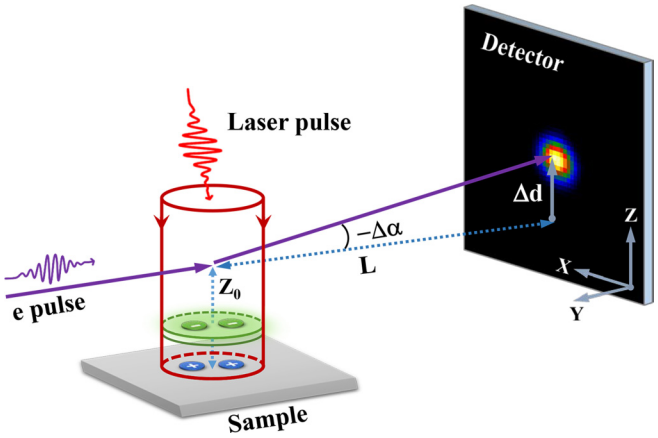

FIG. 1. Experimental configuration. The 800-nm-laser pulse was collimated onto the sample in the perpendicular direction. The centroid of the probe electrons was located at $z_0 = 200\,\mu$m above the sample surface. The detector exposure time was 1.5 s at each delay time. The negative sign of the deflection angle, $-\Delta\alpha$, is defined as the probe electron centroid shifts away from its original position (z_0) along the positive direction of Z axis. The excitation laser beam is depicted by the red cylinder, and the formation of TEFs is demonstrated by the charges at the cylinder bottom. The purple line illustrates the trajectory of the probe electron centroid that is deflected by the TEF.

II. EXPERIMENTAL METHOD

The experimental system used in this study has been described previously [12]. Briefly, the 1 kHz, 800 nm, 70 fs, 1 mJ/pulse output from a Ti:sapphire laser was split into two parts. The first part stimulated the sample, while the second part was frequency tripled to 267 nm and used to generate femtosecond electron pulses from a photocathode. These electron pulses were accelerated to 30 keV by a DC electric field and focused onto the sample by a magnetic lens. The delay time between the pump laser pulse and the probe electron pulse was controlled by a linear translation stage. The 100-nm-thick $La_{0.67}Sr_{0.33}MnO_3$ single crystal, grown on $SrTiO_3$ substrate, was placed on a cold finger that could be cooled to 77 K by liquid nitrogen, or studied at room temperature, 300 K.

As illustrated in Fig. 1, the evolution of the transient electric field, above the sample surface, was extracted from the deflection angle of the probe electrons at each delay time. The deflection angle $\Delta\alpha$, was determined by Δd, the shift of the probe electron centroid on the detector, and the distance between the LSMO sample and detector L, through the relation: $\Delta\alpha = \Delta d/L$ $(L = 46\,cm \gg \Delta d)$. Meanwhile, the experimentally observed $\Delta\alpha$ was correlated with the transient electrical field strength at each delay time through

$$\Delta\alpha = \frac{\Delta V_z}{V_e} = \frac{q\overline{E}_z t}{mV_e} = \frac{q\overline{E}_z t}{m_e V_e/\sqrt{1 - V_e^2/c^2}}, \qquad (1)$$

where ΔV_z is the electron velocity change along the sample's normal direction Z; V_e is the velocity of the 30 keV probe electrons; q is the elementary electron charge; $\overline{E}_z$ the averaged electric field strength sensed by the probe electrons; c is the speed of light; m and m_e are the relativistic and rest mass of an electron, respectively. t is the time required for the probe electrons passing through the pump laser beam diameter. For the 300 and 77 K experiments, the passing time was determined to be 6 and 4 ps, respectively, according to the pump beam diameters.

III. RESULTS AND DISCUSSION

The time-dependent deflection angles are shown in Fig. 2, where the time zero was defined by the first observable change in $\Delta\alpha$. In general, deflections of the probe electrons can be described by three consecutive steps: (1) the electron deflection angle reaches its negative maximum during the first few tens of picoseconds; (2) the electron deflection angle reaches its

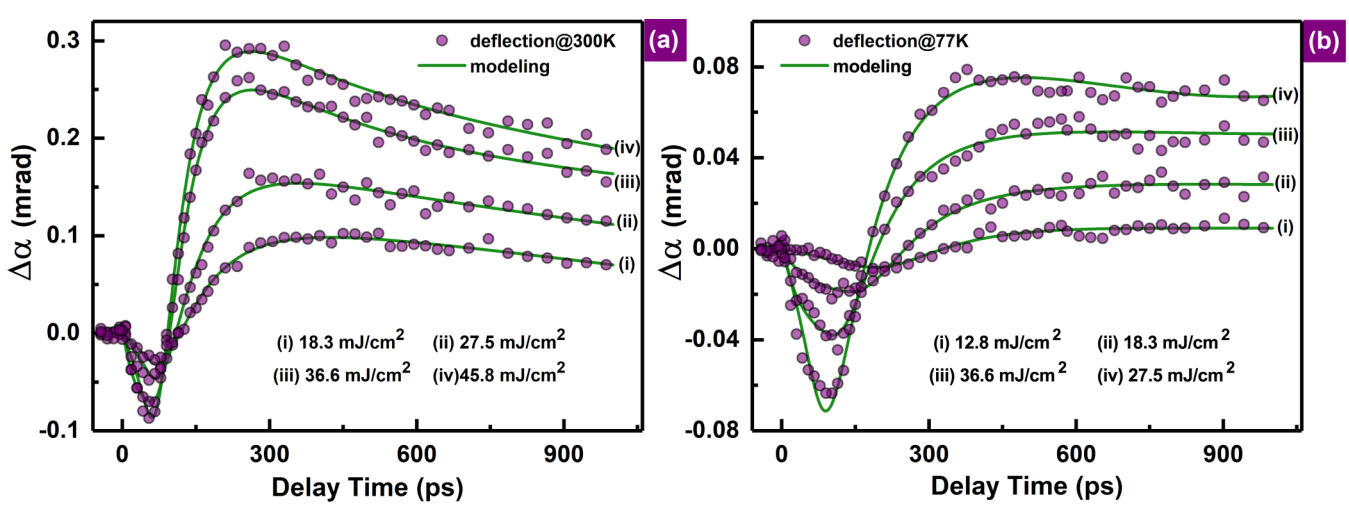

FIG. 2. Time-dependent evolution of probe electron deflection angles due to the charge emission of the laser-irradiated LSMO sample at (a) 300 K and (b) 77 K. The deflection data were reconstructed and plotted using a "three-layer" model, which is introduced in later section of this paper.

positive maximum after a few hundred picoseconds; (3) the deflection angle recovers toward its original position before time zero, which requires more than 900 ps. Such a long recovery time is probably due to experimental bias, or the slow neutralization of the sample. For both temperatures, the negative and positive maxima, increase as a function of laser irradiation fluence owing to the increased number of emitted electrons. At the same time, the characteristic times needed to reach those maxima deflections decreased as the TEF become stronger. For the same pump laser fluence, the deflection angles for LSMO samples at 77 K are smaller than that at 300 K, mainly owing to the reduced kinetic energy and number of emitted electrons at lower temperatures. With larger kinetic energy, the emitted electrons are less likely to be attracted back to neutralize the surface ions. Therefore, a larger portion of the initially emitted electrons can eventually become free electrons that will not fall back to the sample and the associated surface TEF is stronger, which will contribute to a larger deflection angle of the probe electrons.

As shown in Fig. 3, the negative deflection angles observed within the first few tens of picoseconds is due to the fact that, the emitted electrons from the LSMO sample are initially below the centroid of probe electrons[see Fig. 3(a)]. Therefore, the probe electrons are deflected away from the sample surface owing to the Coulomb repulsion by those initially emitted electrons. As the emitted electrons keep moving further away from the sample and towards to cross the probe electrons, the probe electron beam bends toward the sample surface owing to the evolution of the TEF it sensed [see Figs. 3(b) and 3(c)]. Accompanying the initially emitted electrons falling back partially and the reduced charge density, the transient electric field decreases, as a function of time, and the electron deflection angles begin to recover. The characteristic time of the observed deflection angle change, is mainly determined by the initial velocity of the emitted electrons that escape from the LSMO sample, immediately after laser excitation. As the laser pump fluence increases, the time required to reach the negative and positive maxima deflections decreases, indicating a higher emitting velocity that contributes to faster electric field evolution.

The time-dependent transient electric field originates from the fast evolution of the electron plasma layer located above the sample surface. For a detailed description of this complex nonlinear process, large-scale numerical simulations are required to describe such many-body interactions. However, it has been shown that the primary features of such fast evolving plasmas can be extracted by means of analytical models in combination with the experimentally determined electric fields [12–14,16]. And, the plasma features, that are extracted, agree will with the large-scale *particle-in-cell* simulations[17]. In order to obtain the general feature of the electron plasma layer in our study, the deflections of the probe electrons, shown in Fig. 2, were reconstructed using a "three-layer" model [12] which classified the charges, that contribute to the electrical fields, into three categories: (1)

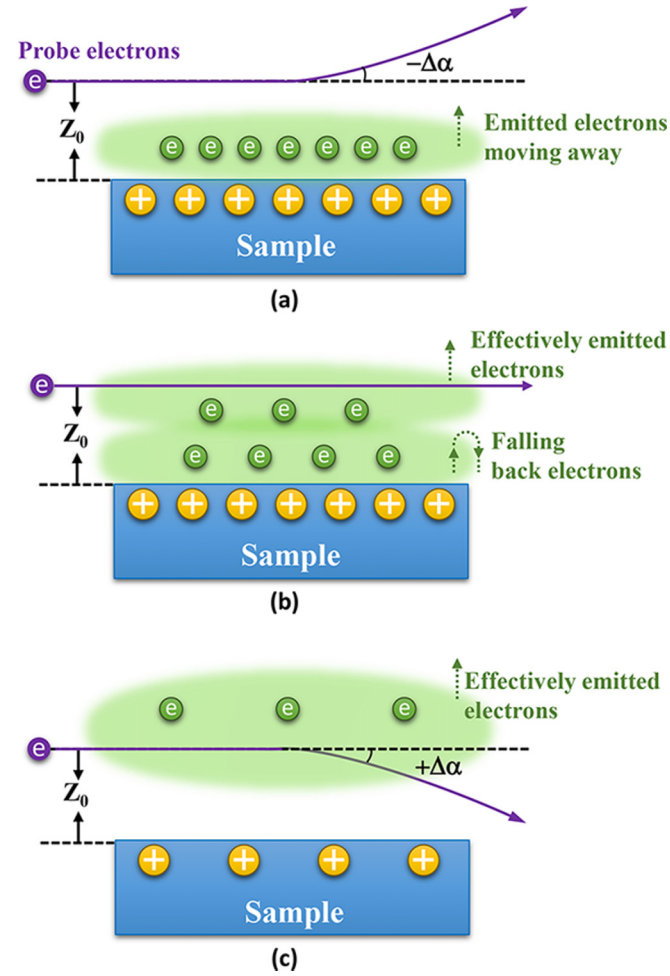

FIG. 3. Schematic representation of the three key stages that the probe electrons are deflected by the surface TEF. (a) Initially, the centroid of the probe electrons is deflected away from the sample surface (the negative deflection angle, Fig. 2); (b) The centroid of the probe electrons were almost unchanged as the emitted electrons partially falling back onto the sample and partially escaping; (c) the centroid of the probe electrons moves toward the sample surface (the positive deflection angle on Fig. 2). The centroid of the probe electron initially locates at z_0 position and its trajectory due to the presence of TEF is marked by a purple line. The electron plasmas due to the emitted charges are marked in green. The three layers of charges that contribute to the TEFs are the surface ions, the "fallen back" electrons, and the effectively emitted electrons.

the positive ions that remained at the sample surface; (2) the "fallen back" electrons, which initially escaped from the sample surface but eventually fell back onto it and partially neutralized the positive ions; (3) the effectively emitted electrons that escaped from the sample and do not fall back. It is worthy to mention that the term "fallen back" indicates neutralization due to electric attractions and it is not an effect of gravity. The contribution of those, different types of charges, to the electric field at position z_0 above the sample is described by Eq. (2)

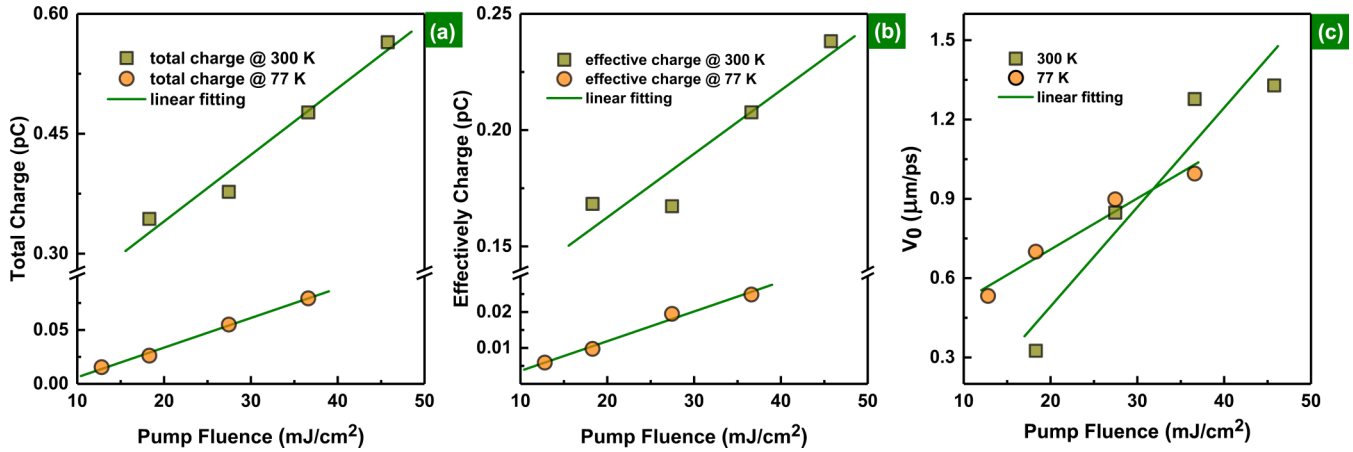

FIG. 4. (a) Total charges emitted at time zero, (b) the effectively emitted charges and (c) the averaged initial velocity of the emitted electrons, V_0, at time zero, as a function of pump laser fluence for LSMO single crystal films at 77 K and 300 K.

[12]:

$$E_z(z_0,t) = \frac{\sigma_0}{2\epsilon_0}\cdot\left\{\left[1-\frac{Z_0}{\sqrt{Z_0^2+(D/2)^2}}\right]\cdot\left[1-\int_{-\infty}^{0}\rho(z,t)dz\right]-\int_0^{z_0}\rho(z,t)\left[1-\frac{z_0-z}{\sqrt{(z_0-z)^2+(D/2+\upsilon_w t)^2}}\right]dz\right.$$
$$\left.+\int_{z_0}^{+\infty}\rho(z,t)\left[1-\frac{z-z_0}{\sqrt{(z_0-z)^2+(D/2+\upsilon_w t)^2}}\right]dz\right\}, \quad (2)$$

In which, σ_0 and ϵ_0 are the area charge density of the initially emitted electrons at time zero and the electrical permittivity of vacuum, respectively; D is the diameter of the positive ions at the surface; owing to space charge effect, the emitted electron plasmas are assumed to expand with velocity υ_w in a direction parallel to the sample surface. The distribution of electrons along the sample, in a direction normal to the surface, is described by the distribution function $\rho(z,t) = (1-\alpha)\rho^E(z,t)+\alpha\rho^F(z,t)$. The two Gaussian distribution functions, $\rho^E(z,t)$ and $\rho^F(z,t)$, whose peak positions change versus time, are used to describe the charge densities of the effectively emitted electrons and fallen-back electrons, respectively. The ratio of the fallen-back electrons to the initially escaped total charges is designated as α ($0 \leqslant \alpha \leqslant 1$). The combination of Eqs. (1) and (2) provide an excellent reconstruction of the deflection angles, which is depicted as the modeling lines in Fig. 2. The primary features of the emitted electrons, obtained through the three-layer model, are (1) the total charges emitted immediately after laser excitation, (2) the electrons that are effectively emitted, and (3) the initial velocity of the emitted charges from the sample surface,which are shown in Fig. 4.

The initial velocity of the emitted electrons shows that, as the laser fluence increases, the kinetic energy of the electrons becomes larger, mainly indicating that thermionic emission is involved. This is also supported by the results from a log-log plot of the total emitted electrons, which has a slope of smaller than 2.0 and indicates multiphoton emission is not evident [12]. The emitting electron velocities mainly determine the evolution of the TEFs, namely, the characteristic time that the probe electrons deflect into their positive and negative maxima. For both temperatures, but at different pump fluencies, the total charges and the effectively emitted charges, deduced using the three-layer model, indicate that more than 50% of the charges, initially emitted at time zero, eventually fall back onto the LSMO crystal where they partially neutralize the surface ions, because of Coulomb repulsions inside the emitted electron charges and attractions from the positive surface ions. As shown in Fig. 4, the slope of the 300 K experiments is larger than that observed for the 77 K experiments. This fact may be due to the reduced thermionic emission as a result of the lower temperature. Utilizing the parameters, obtained by using the three-layer model, to the experimental deflection data, we reconstructed the spatial-temporal distributions of the TEFs above the LSMO surface for the 36.6 mJ/cm^2 laser excitation fluence and illustrated them in Fig. 5.

As shown in Fig. 5(a), in a few picoseconds after the fs pump laser pulse strikes the LSMO surface, the TEF strength may reach 100 kV/m above the surface of the room temperature LSMO crystal. This field strength is on the same order as the THz fields that were used to manipulate charge-orbital couplings in lanthanum strontium manganite [11]. In that study, the orbital domain of a $La_{0.5}Sr_{1.5}MnO_4$ thin film was manipulated by the change of the THz pulse polarization. It was also concluded that, in such domain alignments, the effect of peak electric field strength is more important than the total energy of a THz pulse. Although a strong transient electric field, on the order of hundreds kV/m, may be generated on the surface of room-temperature LSMO films, a smaller transient electric field, on the order of few tens of kV/m, is

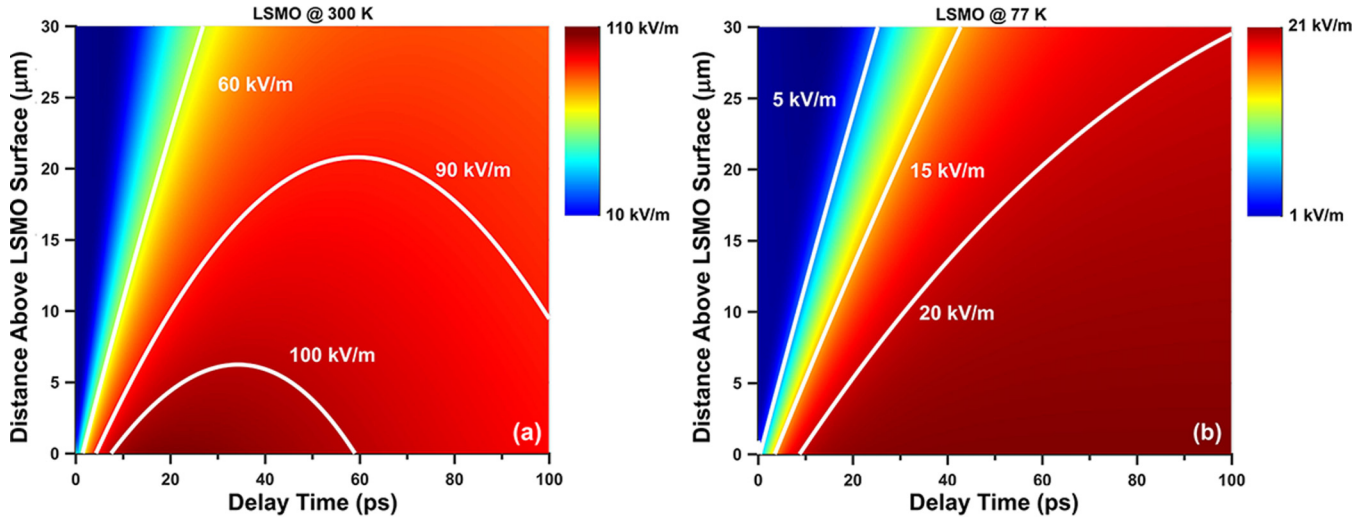

FIG. 5. The spatial-temporal distribution of transient surface electric field strengths that are reconstructed using the three-layer model. The LSMO temperature is (a) 300 K and (b) 77 K and the excitation laser fluence is 36.6 mJ/cm^2.

expected for films at 77 K. However, there are several possible means by which one can increase the strength of TEFs for low-temperature LSMO samples. These include adjusting the doping-levels which increases the electron density [18], or by exciting the sample with higher laser fluence. It is also worth mentioning that, due to the space charge effects (Coulomb repulsion), the electrons that initially escaped from the sample surface will suppress the subsequent electron emissions at a later time [19]. At a certain saturation point, the transient surface electric field strength may not increase as the free electron density or laser illumination intensity become larger. In such a circumstance, utilizing a bias voltage or a specially engineered film may provide a means to further increase the TEF strength [20].

IV. CONCLUSION

In conclusion, the strength and evolution of transient surface electric fields, generated by femtosecond-laser-induced charge emission on LSMO films at 300 K and 77 K temperatures, have been studied by the deflection of femtosecond electron pulses. The experimental data were subjected to a three-layer theoretical model, which revealed the initial velocities and the amount of emitted charges during the laser-induced emission process, and reproduced the evolution of probe electron deflection angles. The spatial-temporal distributions of the surface transient electric fields, reconstructed by the combination of experimental data and the three-layer model, indicates that more than 100 kV/m transient electric fields have been generated. The strength of this electric field is on the same order of magnitude as that used in THz control of complex oxide materials. This study suggests that the transient surface electric fields, generated by femtosecond-laser-induced charge emission, may serve as a potential means for the ultrafast control of materials such as ferroelectricity or generating hidden states.

ACKNOWLEDGMENTS

We are grateful for the technical assistance of A. Krishnamoorthi. This research was supported in part by the National Natural Science Foundation of China (Grants No. 11675106, No. 11721091, No. 11674227, and No. 11704246), the Welch Foundation (Grant No. 15-01928), Air Force Office of Scientific Research (Grant No. FA9550-18-1-0100) and Texas A&M University TEES funds.

[1] E. Dagotto, Complexity in strongly correlated electronic systems, Science **309**, 257 (2005).

[2] H. Zhang, K. Wang, Y. Zhang, W. Dong, L. Chen, X. Tang, and J. Chen, Strong influence of polaron-polaron interaction on the magnetoresistance effect in $La_{0.7}A_{0.3}MnO_3$ thin films, Appl. Phys. Lett. **111**, 192408 (2017).

[3] R. D. Averitt and A. J. Taylor, Ultrafast optical and far-infrared quasiparticle dynamics in correlated electron materials, J. Phys.: Condens. Matter **14**, R1357 (2002).

[4] J. Zhang and R. D. Averitt, Dynamics and control in complex transition metal oxides, Annu. Rev. Mater. Res. **44**, 19 (2014).

[5] C. Giannetti, M. Capone, D. Fausti, M. Fabrizio, F. Parmigiani, and D. Mihailovic, Ultrafast optical spectroscopy of strongly correlated materials and high-temperature superconductors: a non-equilibrium approach, Adv. Phys. **65**, 58 (2016).

[6] C. H. Matthias and F. József András, Intense ultrashort terahertz pulses: generation and applications, J. Phys. D: Appl. Phys. **44**, 083001 (2011).

[7] D. Nicoletti and A. Cavalleri, Nonlinear light-matter interaction at terahertz frequencies, Adv. Opt. Photon. **8**, 401 (2016).

[8] S. Bonetti, M. C. Hoffmann, M. J. Sher, Z. Chen, S.-H. Yang, M. G. Samant, S. S. P. Parkin, and H. A. Dürr, THz-Driven

Ultrafast Spin-Lattice Scattering in Amorphous Metallic Ferromagnets, Phys. Rev. Lett. **117**, 087205 (2016).

[9] F. Chen, Y. Zhu, S. Liu, Y. Qi, H. Y. Hwang, N. C. Brandt, J. Lu, F. Quirin, H. Enquist, P. Zalden, T. Hu, J. Goodfellow, M. J. Sher, M. C. Hoffmann, D. Zhu, H. Lemke, J. Glownia, M. Chollet, A. R. Damodaran, J. Park, Z. Cai, I. W. Jung, M. J. Highland, D. A. Walko, J. W. Freeland, P. G. Evans, A. Vailionis, J. Larsson, K. A. Nelson, A. M. Rappe, K. Sokolowski-Tinten, L. W. Martin, H. Wen, and A. M. Lindenberg, Ultrafast terahertz-field-driven ionic response in ferroelectric $BaTiO_3$, Phys. Rev. B **94**, 180104(R) (2016).

[10] X. Li, T. Qiu, J. Zhang, E. Baldini, J. Lu, A. M. Rappe, and K. A. Nelson, Terahertz field-induced ferroelectricity in quantum paraelectric $SrTiO_3$, Science **364**, 1079 (2019).

[11] T. A. Miller, R. W. Chhajlany, L. Tagliacozzo, B. Green, S. Kovalev, D. Prabhakaran, M. Lewenstein, M. Gensch, and S. Wall, Terahertz field control of in-plane orbital order in $La_{0.5}Sr_{1.5}MnO_4$, Nat. Commun. **6**, 8175 (2015).

[12] R.-Z. Li, P. Zhu, L. Chen, T. Xu, J. Chen, J. Cao, Z.-M. Sheng, and J. Zhang, Investigation of transient surface electric field induced by femtosecond laser irradiation of aluminum, New J. Phys. **16**, 103013 (2014).

[13] H. Park and J. M. Zuo, Direct measurement of transient electric fields induced by ultrafast pulsed laser irradiation of silicon, Appl. Phys. Lett. **94**, 251103 (2009).

[14] R. K. Raman, Z. Tao, T.-R. Han, and C.-Y. Ruan, Ultrafast imaging of photoelectron packets generated from graphite surface, Appl. Phys. Lett. **95**, 181108 (2009).

[15] H.-B. Lu, K.-J. Jin, Y.-H. Huang, M. He, K. Zhao, B.-L. Cheng, Z.-H. Chen, Y.-L. Zhou, S.-Y. Dai, and G.-Z. Yang, Picosecond photoelectric characteristic in $La_{0.7}Sr_{0.3}MnO_3$ p-n junctions, Appl. Phys. Lett. **86**, 241915 (2005).

[16] L. Chen, R. Li, J. Chen, P. Zhu, F. Liu, J. Cao, Z. Sheng, and J. Zhang, Mapping transient electric fields with picosecond electron bunches, Proc. Natl. Acad. Sci. **112**, 14479 (2015).

[17] W. Wendelen, B. Y. Mueller, D. Autrique, B. Rethfeld, and A. Bogaerts, Space charge corrected electron emission from an aluminum surface under non-equilibrium conditions, J. Appl. Phys. **111**, 113110 (2012).

[18] J. Hemberger, A. Krimmel, T. Kurz, H.-A. Krug von Nidda, V. Y. Ivanov, A. A. Mukhin, A. M. Balbashov, and A. Loidl, Structural, magnetic, and electrical properties of single-crystalline $La_{1-x}Sr_xMnO_3(0.4 < x < 0.85)$, Phys. Rev. B **66**, 094410 (2002).

[19] W. Wendelen, B. Y. Mueller, D. Autrique, A. Bogaerts, and B. Rethfeld, Modeling ultrashort laser-induced emission from a negatively biased metal, Appl. Phys. Lett. **103**, 221603 (2013).

[20] Q. Weng, S. Komiyama, L. Yang, Z. An, P. Chen, S.-A. Biehs, Y. Kajihara, and W. Lu, Imaging of nonlocal hot-electron energy dissipation via shot noise, Science **360**, 775 (2018).